

Simulation Standard

QUANTUM: Quantum Mechanical Simulator Released in ATLAS

Introduction

Silvaco has recently released QUANTUM, a 2D quantum mechanical solver coupled into the poisson, drift diffusion and energy balance solvers already available in ATLAS. The physics of quantum mechanics have been included to model the behavior of heterojunction devices which exhibit properties such as quantized channel confinement and transmission or reflection at potential barriers. The model has been implemented for both electrons and holes. This allows more accurate physically based simulations of devices such as pseudomorphic HEMTs, as illustrated in Figure 1. An additional feature arising from this work has been the ability to simulate quantized MOS channels and shifted CV curves for thin oxide sub-quarter-micron devices.

Implementation

The two techniques that have been studied at Silvaco for the inclusion of quantum mechanical effects are a coupled Schrodinger-Poisson approach and a coupled Quantum moments technique.

Initial investigations centered around the implementation of a Schrodinger-Poisson system - in this technique, the Schrodinger equation is solved in two sections using the Sturm sequence approach to calculate the required eigen values and corresponding eigen vectors [1]. The eigen values represent discrete energy level subbands, in which electrons can reside. The eigen vectors give the probability of occupation of a given energy level for the particular bias conditions applied. This provides useful information in terms of how quantum mechanics is affecting the electron distribution within the device, and where the sub-bands occur. The implementation of this system is included in the December 1996 issue of the Simulation Standard. The main problem with this type of approach for a device simulator is that the quantum solution does not take into account the impact of quantum mechanics on the transport equations.

An alternative method of incorporating the effects of quantum behavior within a device simulator is to use the Quantum Moments approximation technique [2]. This technique uses an additional term on the transport

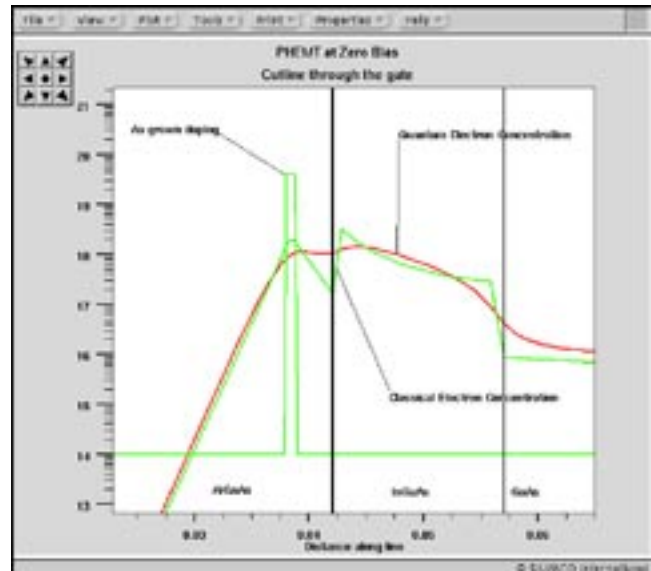


Figure 1. Delta doped PHEMT - cutline through the gate showing smearing of the electron concentration in the quantum model as compared to classical.

equations which allows for the repositioning of carriers under the influence of quantization, using a quantum temperature, as illustrated in equation (1):

$$U_q = -\frac{\hbar^2}{6m^*} \nabla^2 \ln(n)$$

where \hbar and m^* are the reduced planck constant and effective mass, n is the electron concentration and U_q is the quantum term incorporated into the transport equations.

The quantum moments equation, which provides explicit quantum corrections, is based upon the second moments of the Wigner function [3].

Continued on page 2....

INSIDE

| | |
|-----------------------------------------------------------------|----|
| SIMS-Verified Implant Models Released in ATHENA 4.3 | 4 |
| Modifications and Additions to the Ferroelectric Model in Atlas | 8 |
| Calendar of Events | 10 |
| Hints, Tips, and Solutions | 11 |

Heterojunction Applications

The main application area for this type of model is in III-V heterojunction device structures, and to illustrate this, examples of a HEMT, PHEMT and heterojunction diode will be given.

Figure 2 shows a typical HEMT type structure with AlGaAs / GaAs layers. A cutline is shown through the gate illustrating the electron concentration for both the classical and quantum solutions. The quantum smoothing out of the classical concentration peak in the channel is clear from this figure, as is the increase of the carriers on the other side of the barrier.

Figure 1 (on the previous page) shows a PHEMT with an AlGaAs / InGaAs / GaAs structure. Again a cutline has been taken through the channel - this device has a delta (pulse) doping in the AlGaAs layer. The effects of the quantum model can be seen in the differences between the doping concentration and the electron concentration. Clearly the delta pulse has been 'smeared out' and the carriers are located in the channel potential well. Figure 3 shows an Id/Vd curve for this device showing the standard types of result that can be produced with a quantum based model.

A simple heterojunction diode is shown in Figure 4, including the conduction and valance bands from anode to cathode. Figure 5 shows the electron concentration within this device for both classical and quantum structures. Again, the shift from sharp classical peaks can be seen in the quantized results, with a higher carrier concentration on the other side of the barrier. In Figure 6, the difference that this makes to the reverse current can be seen - the quantum case gives a higher leakage current in the device.

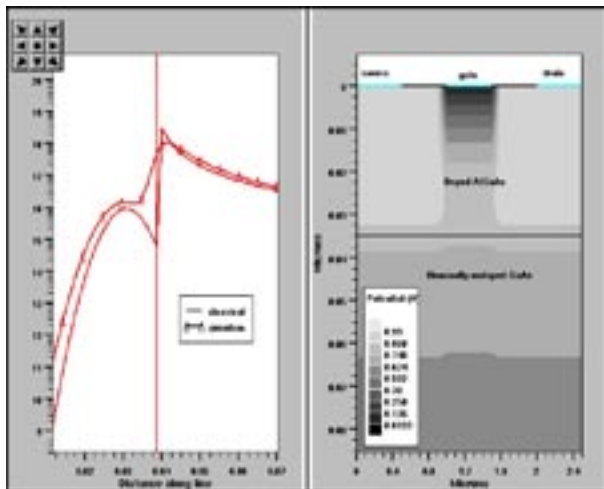


Figure 2. Quantum and classical carrier concentration for a HEMT structure.

MOS Applications

Another set of applications are for ultr thin gate MOS structures. QUNATUM accounts for quantization effects in a MOS channel. This leads to changes in CV curves with thin gate oxides. Note that in this type of simulation

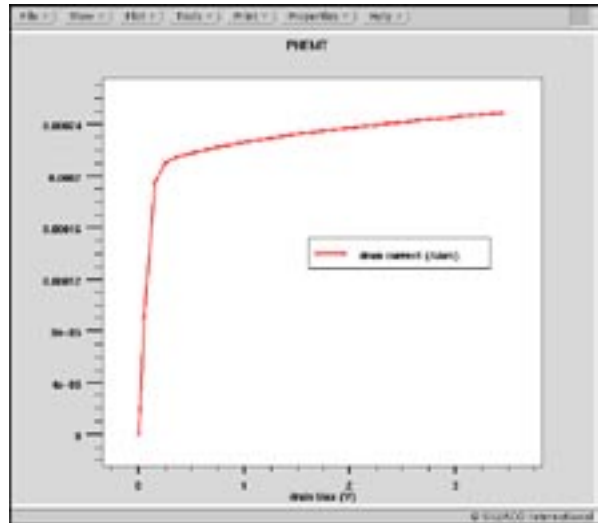


Figure 3. Id/Vd curve at $V_g=0V$ for a HEMT using QUANTUM. Note the correct prediction of conductor current levels.

we are using a physical description of what exactly is happening to the carrier, and therefore modeling the behavior of this phenomena accurately. This contrasts to other approximate methods for including quantum effects which use an empirical adjustment to Poisson equation. Figure 7 illustrates the device simulated and the classical verses quantum carrier concentration through the gate. Note the reduction in carrier concentration towards the surface of the device - this is typical of a quantized device and leads to the shift in CV characteristics shown in Figure 8 as the inversion layer is less inverted than in the classical case. Additionally, Figure 9 shows the classical and quantum n_i - illustrating the surface dip due to quantization. The quantization of holes is possible in QUANTUM which allows the simulation of both NMOS and PMOS structures.

Conclusion

Silvaco has released QUANTUM, a quantum model within the framework of our existing 2D device simulator ATLAS. This is based on a quantum moments ap-

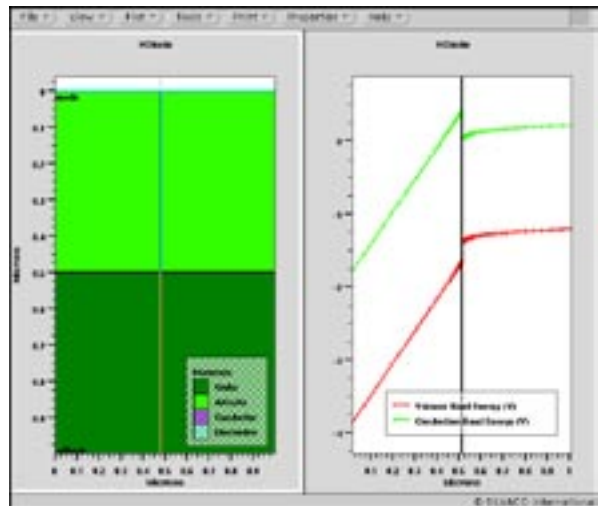


Figure 4. AlGaAs/GaAs heterojunction diode.

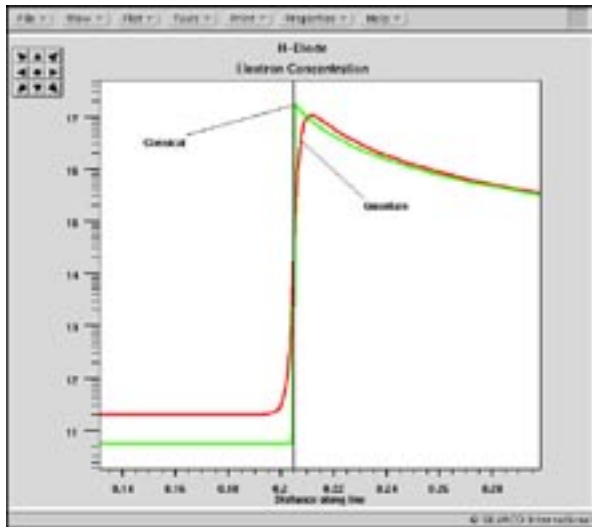


Figure 5. Electron concentration across the junction in reverse bias.

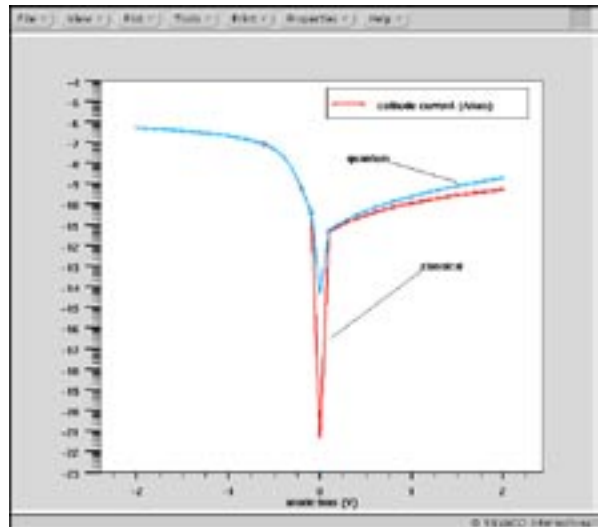


Figure 6. Heterojunction diode forward and reverse bias currents. Extra current in quantum case is due to smoothing of electron concentration across the heterojunction.

proximation derived from the second order moments of the Wigner function. The incorporation of this type of model allows more accurate, physically based simulation of quantized channel devices, in particular III-V HEMTs and heterojunction diodes, but is also applicable to sub quarter-micron MOS devices.

References

- [1] R. Drury and C. Snowdon, "A Quasi-2D HEMT Model for Microwave CAD Applications," IEEE Trans. Electron Devices, vol. 42 no. 6, pp 1026, 1995
- [2] Jing-Rong Zhou and David Ferry, "Simulation of Ultra-Small GaAs MESFETs Using Quantum Moment Equations," IEEE Trans. Electron Devices, vol. 39 no. 3, pp 473, 1992
- [3] E. Wigner, "On the Quantum correction for thermal dynamic equilibrium," Phys. Rev., vol. 40 no. 5, pp. 749-754, 1932

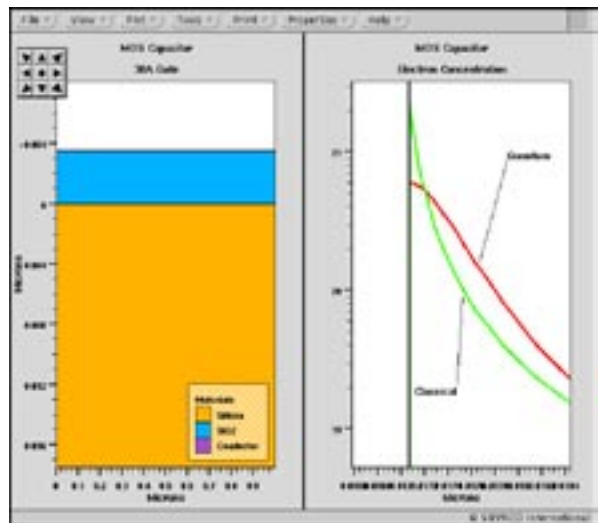


Figure 7. MOS capacitor structure with 30Å gate oxide. Channel quantization reduces the surface carrier concentration.

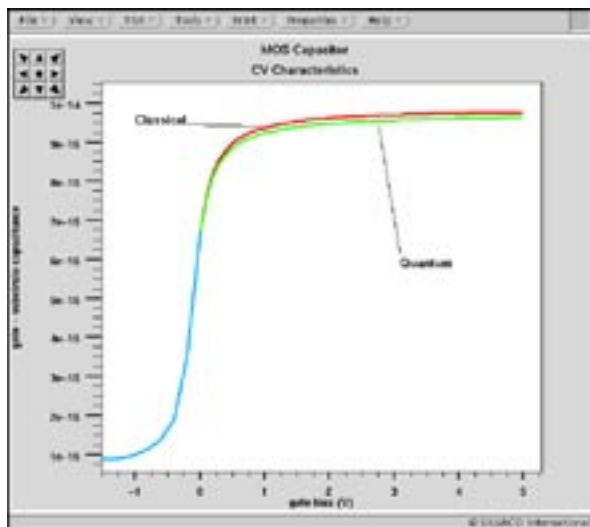


Figure 8. CV curves illustrating a shift due to quantization. The shift leads to erroneous T_{ox} measurements of ultra-thin gate oxides.

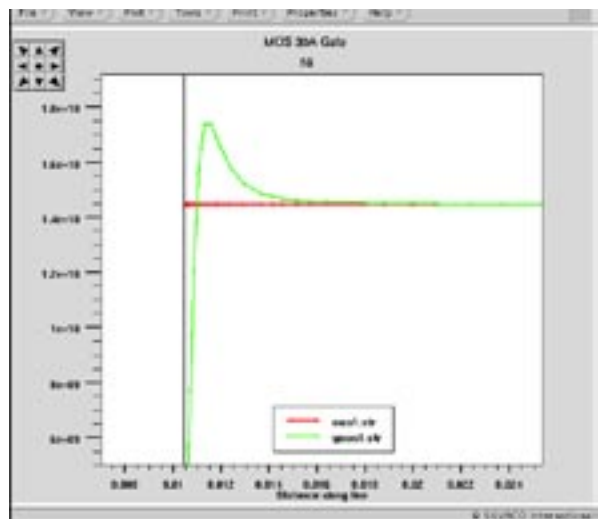


Figure 9. Ni for classical and quantum cases showing non-uniform N_i in quantized regions.

SIMS-Verified Implant Models Released in ATHENA 4.3

ATHENA version 4.3 has been released containing significant developments in implantation and lithography simulation. The implantation improvements compliment the developments made in diffusion and RTA models released last year in ATHENA version 4.0. This combination of advanced implant and diffusion models provide a complete solution to simulation of deep sub-micron processes. The lithography developments allow Optical Proximity Correction (OPC) simulation for complex masks.

New SIMS-Verified Dual Pearson (SVDP) Implant Models

The importance of accurate implant simulation has increased in recent years as thermal processing is reduced for sub-half micron processes. Modern diffusion models such as those released last year in ATHENA 4.0 require that the as-implanted profiles are highly accurate. This because the implant damage, the driving force behind RTA effects, has been consistently shown in research to be scaled to the doping profile through the UNIT.DAMAGE (or PLUS.ONE) model.

A new SIMS Verified Dual Pearson (SVDP) model has been implemented. This model is based on experiments and research conducted by Professor Al Tasch and co-

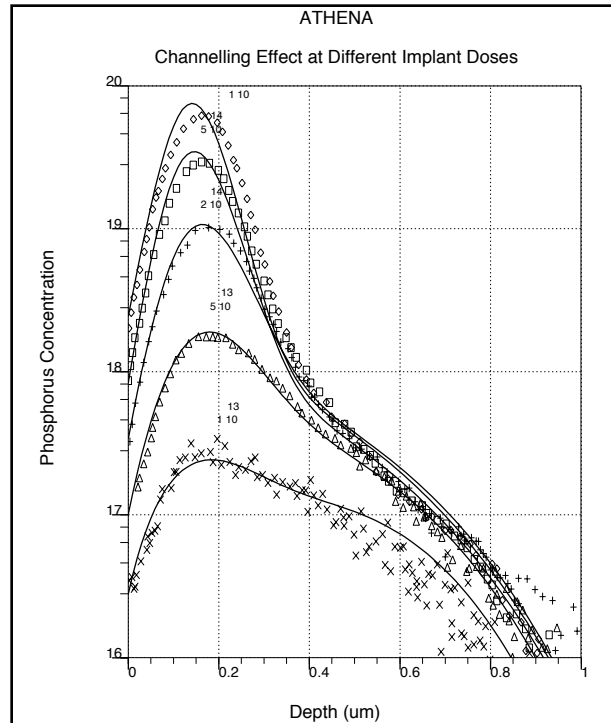


Figure 1. Dose dependence of phosphorus implants along <100> channel in Si.

Curves - ATHENA simulations using the SVDP model, Experimental points R.J. Schreutelkamp et.al., Nucl. Instr. Meth. B55, 615 (1991)

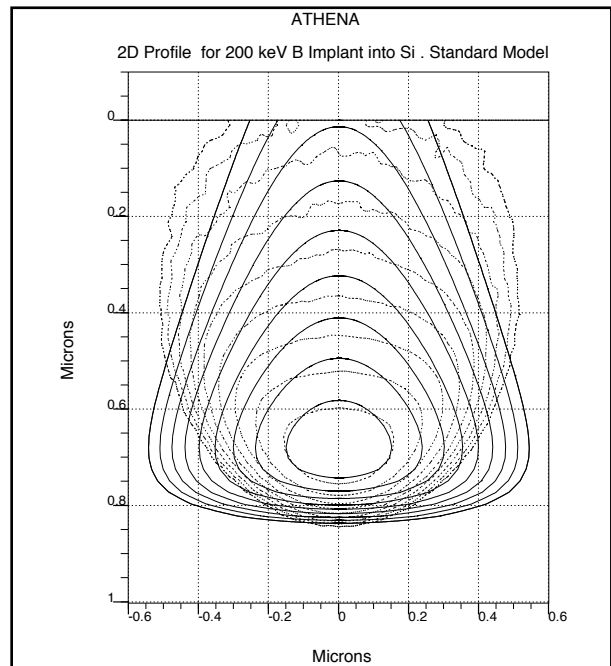
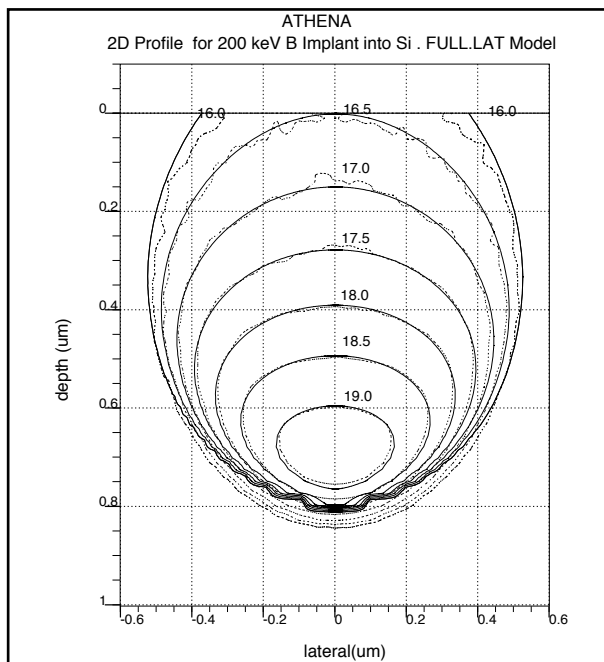


Figure 2. Simulated 2D profiles for 200 keV B implant into amorphous Si are shown in Figure 2a. The solid contours are the FULL.LAT analytical model, dashed contours are Monte Carlo simulation. Implantation takes place at the point (0,0) in the vertical direction downwards. Figure 2b is the same as Figure 2a, with the standard analytical model is used showing poor agreement.

workers in the University of Texas at Austin[1]. The model provides analytical implant tables that describe:

- **dual pearson distributions to describe channeling for B, BF₂, P and As**

Older models contained dual pearson distributions only for Boron. Channeling for P and As is significant at low tilt angles.

- **tilt angle dependence of channeling profile**

The new implant tables contain separate implant moments from measured data for several tilt angles. Interpolation between tilt angles is done by the model. Previous model used a simple cosine relationship to describe the range as a function of tilt angle.

- **dose dependent channeling**

The new tables have dose dependent moments that are especially apparent in the reduction of channeling in high dose source/drain implants when compared to lower doped LDD implants. (See Figure 1.)

- **Screen oxide dependent channeling**

The new tables contain separate implant moments from measured data for several screen oxide thicknesses for Boron. Interpolation between tilt oxide thickness is done by the model. The parameter `S.OXIDE` is used to set the screen oxide thickness. Automation of `S.OXIDE` can be done by measuring the oxide prior to implant and using \$-substitution of the variables.

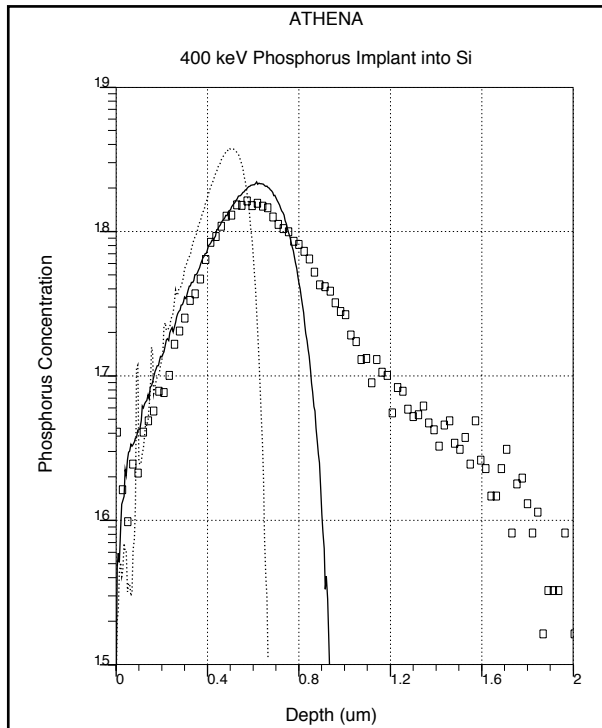


Figure 4. 400 keV Phosphorus Implant into Si.
 Solid curve - Amorphous Monte Carlo Simulation using version 4.3.0.R
 Dashed line - the same using version 4.0.0.R
 Squares - experiment (single crystal silicon, 7 degrees tilt)
 Amorphous MC model matches well to the surface profile and peak. The crystalline MC model is required to match channeling tail

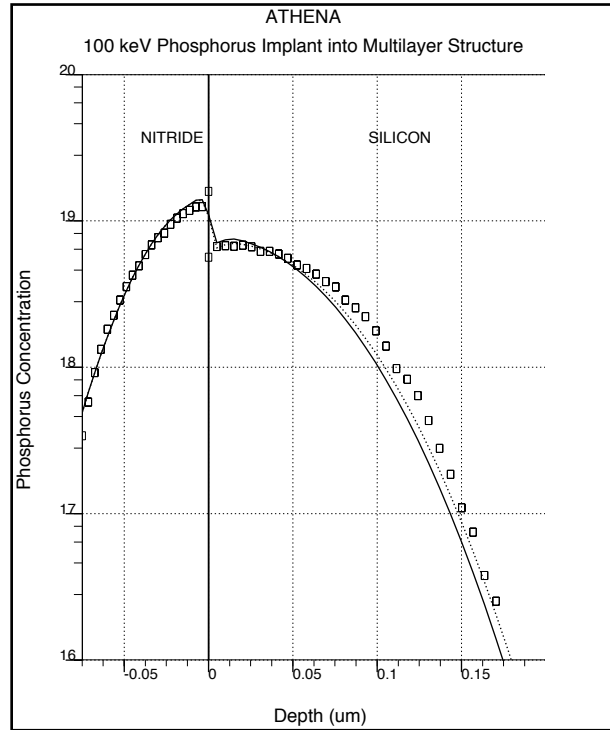


Figure 3. 100 keV phosphorus implant into multilayer structure.
 Solid curve - analytical dose matching method (default);
 Dashed curve - analytical maximal range scaling method (MAX.SCALE);
 Squares - Monte Carlo simulation.

The SVDP implant model is used over a range of dose, energy, tilt, rotation and screen oxide thickness determined by the original research[1]. Outside this range the program uses implant moments from the previous model tables. The parameter `PRINT.MOM` can be used on the implant statement to get explicit data on the implant moments used and their source table.

Modeling of Lateral Implant Range

The `FULL.LAT` model for accurate simulation of 2D implant profiles has been improved. It can now be used together with the SVDP model. It also includes lateral distributions based on symmetrical Pearson functions.

The `MOMENTS` statement functionality has been extended to support the SVDP and improved 2D implant models.

Implantation into Multi-Layer Targets

Two additional models for implants in multi layered structures are added. They are based on the range (`RP.SCALE`) or maximum range (`MAX.SCALE`) scaling. The dose matching model (`DOSE.MATCH`) remains a default. Differences between these models are important when the range of the implant is close to the thickness of a screen layer. (See Figure 3.) The parameter `SCALE.MOM` invokes moments scaling algorithm which can be used with any of above models to scale the default implant moments.

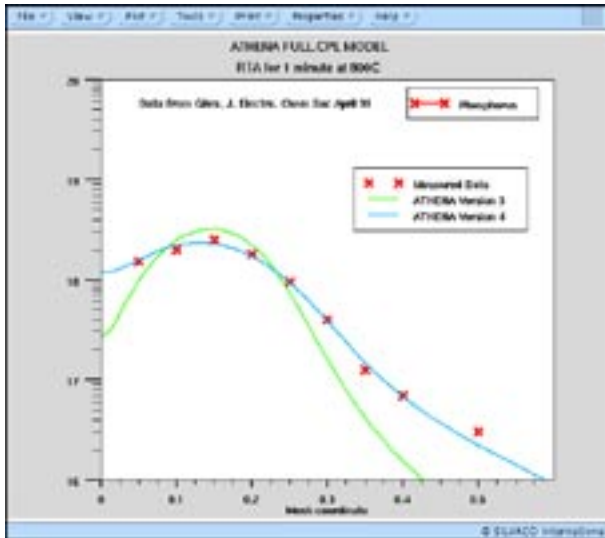


Figure 5. Comparison of *default* diffusion model parameters to measured data. Coefficients in Version 4 based on latest research provide best fit.

Improvements in Monte-Carlo Implantation

Amorphous Monte Carlo Implant Model has been improved. It now uses much more accurate model for electronic stopping which substantially increased the accuracy of MC profiles for intermediate (few hundreds KeV) and high (few MeV) implant energies. In addition non-physical spikes in MC profiles near the surface are eliminated because a more sophisticated free-path-length estimation algorithm is used now. (See Figure 4.)

New parameter IMPCT.POINT allows simulation of point source Monte Carlo implant to produce a 2D distribution. Extraction of spatial moments using parameter PRINT.MOM is also supported in this mode.

Diffusion Simulation Enhancements

In the <311> cluster model[3] used for RTA simulations (CLUSTER.DAM) the decrease of interstitial concentration in <311> clusters during interstitial release is now included. This allows correct simulation of RTA cycles which include several independent temperature steps. (See Figure 5).

The default model file "athenamod" has been updated. It includes better set of parameters for interstitial diffusion and the <311> cluster model. Unlike the FULL.CPL model the CLUSTER.DAM model can predict the transient enhanced diffusion effect over a range of time and temperature with the same default conditions. An example is shown in Figure 6 and 7.

In order to support backward compatibility the model files for two previous versions 4.0 and 3.0 are also available by using commands **athena -modfile 96** and **athena -modfile 95** correspondingly. This allows users with concerns about backwards compatibility to check the new parameter set against the old easily.

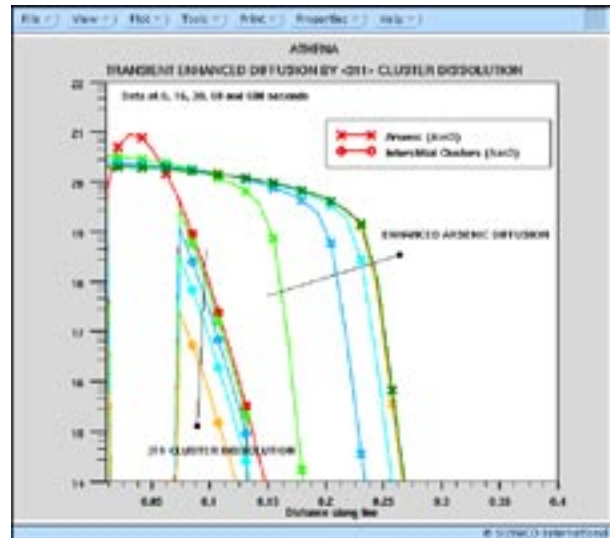


Figure 6. Transient enhanced diffusion of arsenic at 850°C. The 311 clusters dissolve over approx. 60 seconds releasing interstitials to fuel the enhanced diffusion.

A prototype model file is also available using **athena -modfile prototype**. This model file contains parameters collected from recent published research. The effect of these newest parameter sets on typical simulation is still under evaluation. However used parameters from this file can be as a guideline for calibration purposes.

Oxidation Simulation Enhancements

The parameter FLIP.FACTOR has been added to the METHOD statement. It allows to control mesh behavior and improve convergence of oxidation simulation. This parameter varies from zero to one. Changes from the default are recommended only for those cases when oxidation simulation experiences convergence problems.

FLASH Enhancements

C-interpreter capability is implemented for all impurities recognized by FLASH. Parameters DIF.COEF, SEG.CALC, and ACT.CALC in the IMPURITY statement specify the files which contain C-interpreter functions for diffusivity, segregation, and activation of specified impurity in selected material.

Optolith Enhancements

For this release, there are two new features for Optolith. One is the capability for performing optical proximity correction (OPC). This OPC capability is done in conjunction with MASKVIEWS. Details of this feature have been described in the previous issue of Simulation Standard [3] and will not be repeated here.

The other new feature is the pattern on the mask is no longer approximated by upright rectangles. The partitioning of the mask pattern can now be done by using rectangular, triangular and circular shapes with arbitrary orientation. With this flexibility, it will greatly enhance the accuracy and computational speed for the

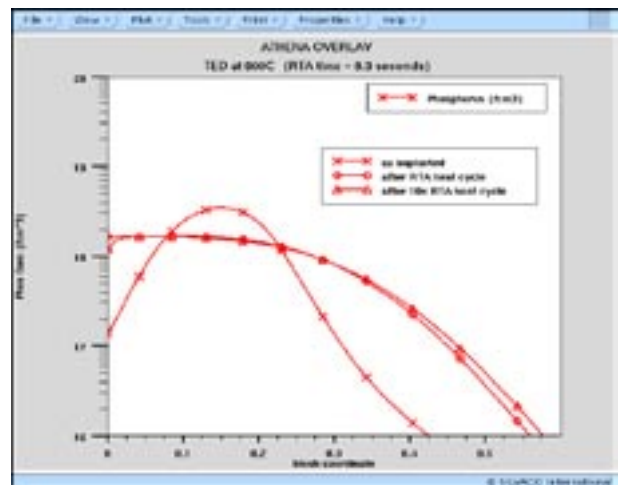
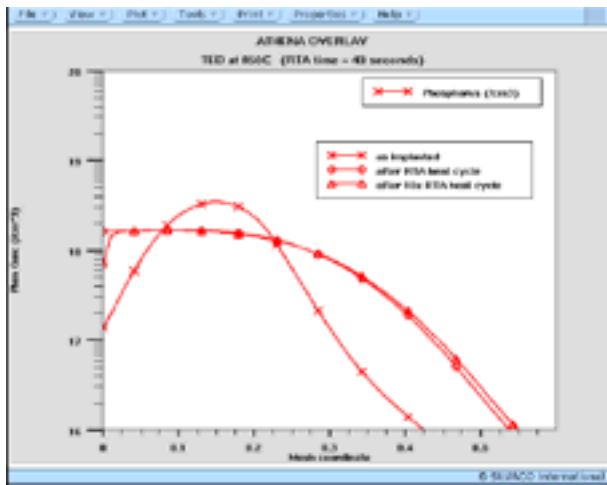
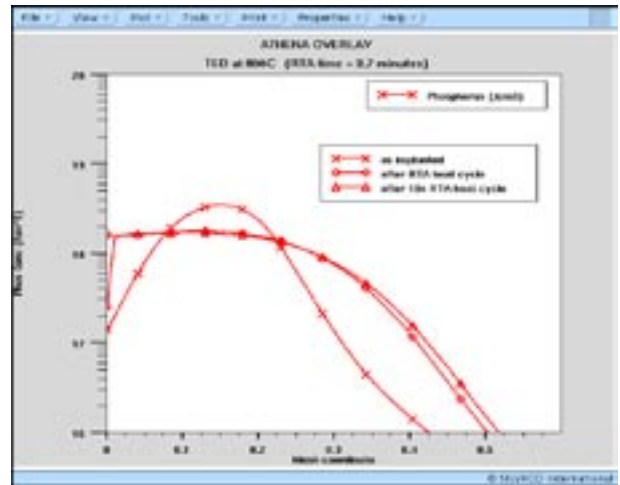
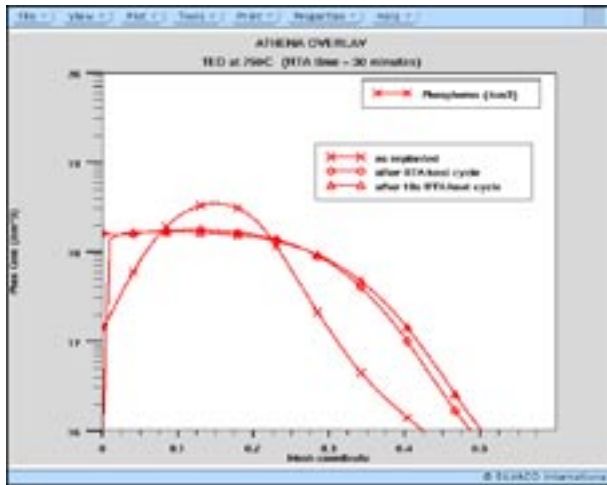


Figure 7. Temperature dependent RTA effects can be modeled using *default* diffusion coefficients in ATHENA 4.3. For each of four temperatures (750°C --> 900°C) simulations are run for a critical TED time documented in [2] and for 10 times the critical time. Results show how long the TED effect lasts at low temperatures.

non-Manhattan geometry, which occurs quite often in the actual layout pattern. The aerial image for a 45(wire joint and a 0.5 mm circular contact opening is displayed in Figure 8. The LAYOUT command has been revised to accommodate these changes, for example,

```
layout x.circle=0.0 z.circle=0.0
      radius=0.25
layout x.lo=1.0 z.lo=-0.75 x.hi=1.3
      z.hi=0.75 rot.angle=0
layout x.tri=1.3 z.tri=0.25 width=0.3 height=0.3
      rot.angle=90
```

The first LAYOUT command describes the 0.5 mm circle at the center. The second LAYOUT command specifies the rectangle at the lower-right corner. The last LAYOUT command draws the triangle adjacent to the previous rectangle. The angle of rotation is specified in degree and is measured with respect to the x-axis.

References

- [1] Simulation Standard Dec 96 "Advanced Analytical Implantation in ATHENA"
- [2] Simulation Standard Aug 96 "TED Modeling in ATHENA"
- [3] Simulation Standard Feb 97 "Performing Optical Proximity Correction in ATHENA"

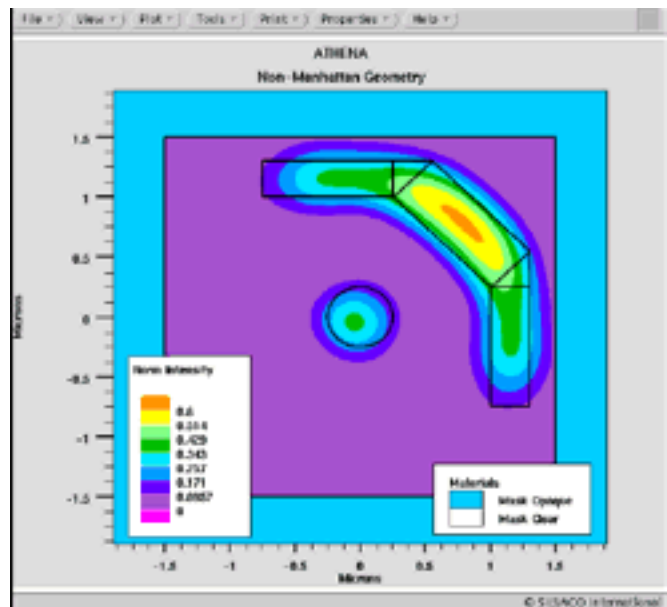


Figure 8. Images from non-rectangular mask shapes can now be simulated in Optolith.

Modifications and Additions to the Ferroelectric Model in Atlas

In the Fall Release 1996 Silvaco International introduced a ferroelectric module as part of the ATLAS device simulation framework. Development work has continued on this module in order to better meet our customers needs. This article reports two modifications to the existing module which are now available in ATLAS.

1. Unsaturated Polarization

It is well understood that in the static or DC state the permittivity of a ferroelectric material is given by

$$\epsilon(E) = \frac{\partial D}{\partial E} = \epsilon_0 \epsilon_f + \frac{\partial P_d}{\partial E}$$

where E is the electric field, D is the displacement vector, ϵ_f is the ferroelectric permittivity and P_d is the position dependent dipole polarization.

The derivative of the dipole polarization with respect to electric field is given by:

$$\frac{dP_d}{dE} = \Gamma \frac{dP_{sat}}{dE}$$

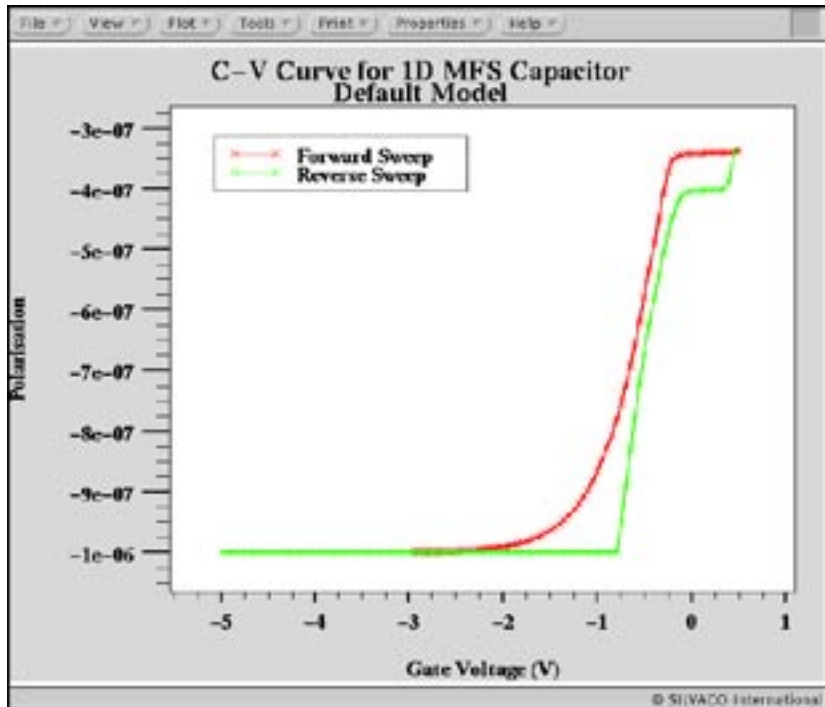


Figure 1. Simulated polarization plot using the default model that illustrates the inaccuracies which arise by assuming saturated polarization.

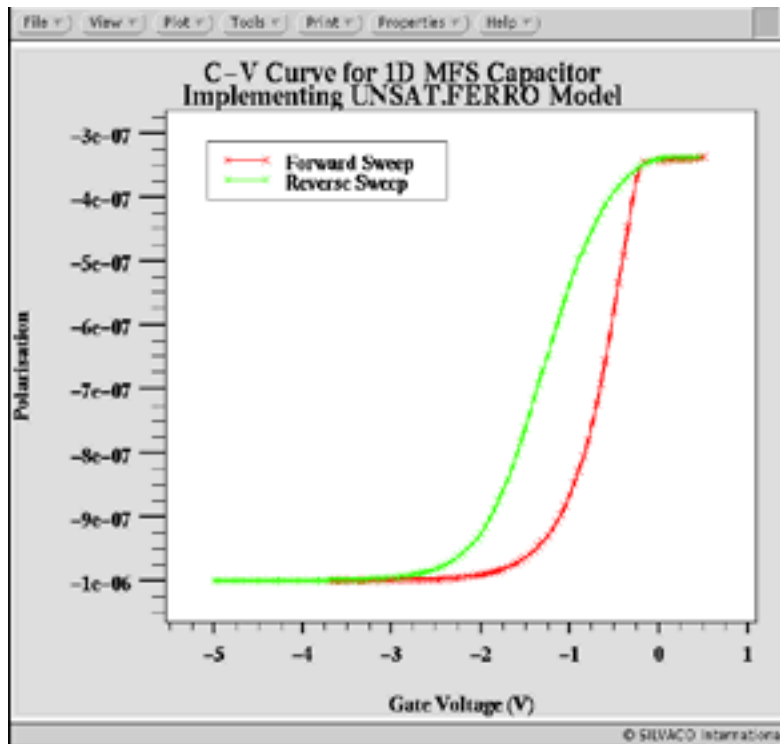


Figure 2. Simulated polarization plot which illustrates that the new improved model for polarization does not require a saturated hysteresis curve to be traced.

where P_{sat} is the position dependent *saturated* dipole polarization. A numeric integration of this function is carried out in Atlas to calculate the position dependent dipole polarization. In the previous release we have assumed that the dipole polarization is saturated. The Ferroelectric model has now been modified to allow the simulation of unsaturated polarization loops as follows.

For saturated loop polarization, the function Γ is unity, which corresponds to the default model. If the user specifies the parameter UNSAT.FERRO on the models statement, the function Γ can take a more general form suitable for the simulation of unsaturated loops. In this case, Γ is given by:

$$\Gamma = 1 - \tanh \left[\left(\frac{P_d - P_{sat}}{\zeta P_s - P_d} \right) \right]$$

where $\zeta = +1$ for increasing fields and $\zeta = -1$ for decreasing fields.

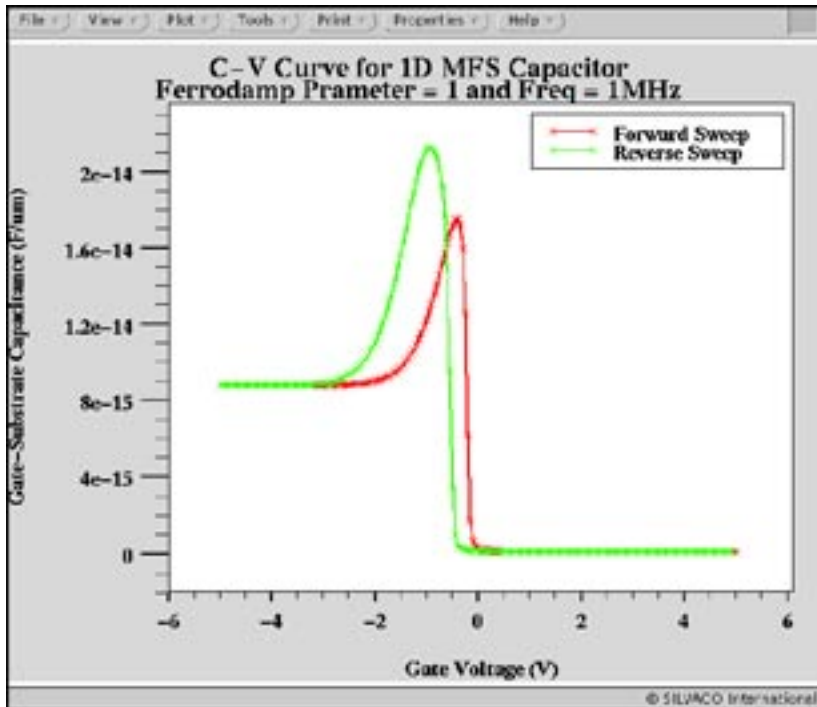


Figure 3. In Figure 2a simulated C-V curve which assumes a dc behavior for permittivity.

This modification to the dipole polarization results in a small but yet significant change in the device simulations. Figures 1 and 2 illustrate this for a one-dimensional MFS capacitor structure where the gate voltage is swept from -5V to +0.5V. The polarization curve is therefore simulated beginning from a saturated position and finishes on an unsaturated position on the polarization curve. Figure 1 shows that with the default model the reverse sweep from +0.5V to -5V the polarization is miscalculated. With the extension of the model to unsaturated regions, shown in Figure 2, the polarization is now correctly calculated for any applied gate voltage sweep.

2. High Frequency Response

Under AC conditions the Ferroelectric material properties can allow the effect of the dipole polarization to have reduced influence on the dielectric permittivity. This effect can be important as, for instance, capacitance C-V curves are normally calculated using a 1 MHz AC signal. It has been suggested that the field dependent polarization has a reduced contribution to the total permittivity, while the hysteresis remains the

same. To include this effect the FERRODAMP parameter has been added to the solve statement. This parameter may have an integer value between 0 and 1, where 0 corresponds to no field dependent polarization and 1 corresponds to the full effect. To illustrate this effect the capacitance curves of the previous MOS capacitor are shown in Figure 3 and 4. The ferrodamper parameter has been used to illustrate that different C-V curves can be obtained. Recent publications seem to indicate that the C-V curve shown in Figure 4 is more realistic. [1]

References

- [1] J-S Lyu et al, "Metal-Ferroelectric Semiconductor Field-Effect Transistor (MFS-FET) for Single Transistor Memory by Using Poly-Si Source/Drain and BaMgF4 Dielectric", IEDM 1997, p. 496.

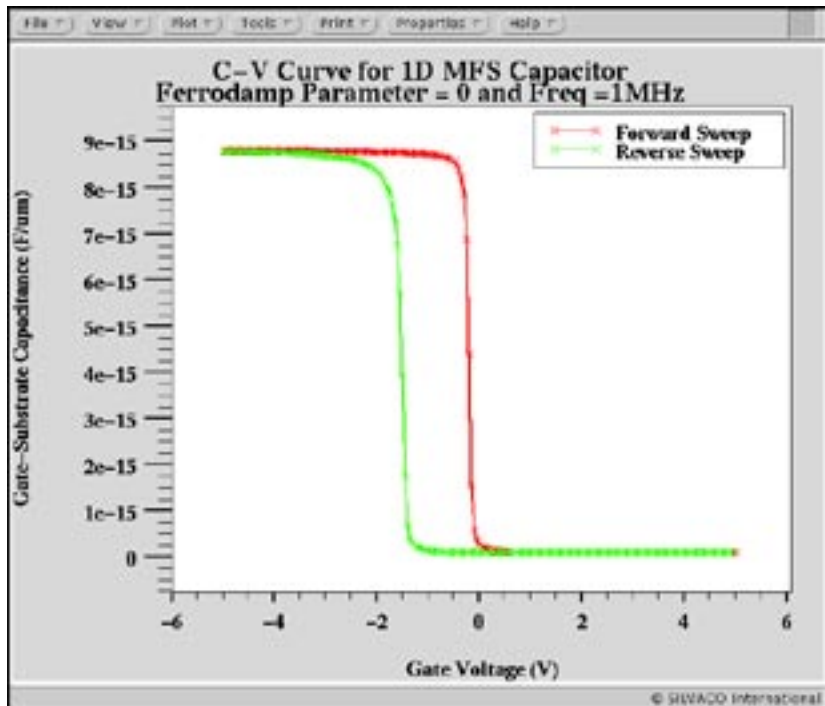


Figure 4. Simulated C-V curve which assumes a high frequency ac, or linear dielectric, behavior for permittivity. This shows that ATLAS can differentiate between low and high frequency behavior.

Calendar of Events

April

| |
|-----------------------------------|
| 1 |
| 2 |
| 3 |
| 4 Workshop - Japan |
| 5 |
| 6 Ultrashallow Junction Symposium |
| 7 Ultrashallow Junction Symposium |
| 8 |
| 9 |
| 10 Workshop - Munich |
| 11 |
| 12 |
| 13 |
| 14 |
| 15 |
| 16 |
| 17 UTMOST Workshop - Japan |
| 18 P/D Workshop - Japan |
| 19 |
| 20 |
| 21 |
| 22 |
| 23 |
| 24 Workshop - Grenoble |
| 25 |
| 26 |
| 27 |
| 28 |
| 28 |
| 30 |

May

| |
|-----------------------------|
| 1 |
| 2 |
| 3 |
| 4 |
| 5 CICC-Exhibition Booth #12 |
| 6 CICC-Exhibition Booth #12 |
| 7 CICC-Exhibition Booth #12 |
| 8 CICC-Exhibition Booth #12 |
| 9 |
| 10 |
| 11 |
| 12 |
| 13 |
| 14 |
| 15 Workshop - Munich |
| 16 |
| 17 |
| 18 |
| 19 |
| 20 Workshop - Guildford |
| 21 |
| 22 |
| 23 |
| 24 |
| 25 |
| 26 ISPSD - Weimar, Germany |
| 27 ISPSD - Weimar, Germany |
| 28 Workshop - Grenoble |
| 28 |
| 30 Workshop - Japan |
| 31 |

Bulletin Board



All Silvaco Offices Report Record Revenues!

Silvaco Japan, Ltd., a wholly owned subsidiary of Silvaco International located in Yokohama, led the way with reported revenues of **\$2.06 million for the quarter**. For the first time, a single sales office broke through the \$2 million sales in a single quarter. Continuing an established pattern of growth, each of Silvaco's ten offices reported sales at record levels. A target set last year to reach \$35 million in sales in 1997 seems achievable.



Visit Silvaco at the DAC show in Anaheim!

1997 DAC show will be held at the Anaheim Convention Center on June 9, 10, 11. Silvaco will be located in booth 1791, Hall C. Silvaco will have a very strong presence and will demonstrate a large array of new products including the pioneering concept of "TCAD Driven CAD."



Exhibition Presentation at the DAC '97 Show

Dr. Ivan Pesic, President of Silvaco International, will present on Monday June 9, at 9:40 a.m. in room B7, a presentation titled: "Tearing Down the Barriers to Sub-Quarter Micron Design."



Silvaco Japan Moves and Expands!

Rapid growth of Silvaco Japan necessitated a move of the offices to much larger quarters. The new office will accommodate a large training room for weekly workshops (for 30 engineers), 50 employees and a large computer center to serve as a computational hub for Silvaco Far East operations. The new address and phone numbers are:

Silvaco Japan
Miyake Building 4F
549-2 Shinano-cho
Totsuka, Yokohama 244
Japan
Phone: (45) 820-3000
Fax (45) 820-3005

For more information on any of our workshops, please check our web site at <http://www.silvaco.com>

The Simulation Standard, circulation 12,000, Vol. 8, No. 4, April 1997 is copyrighted by Silvaco International. If you, or someone you know wants a subscription to this free publication, please call (408) 567-1000 (USA), (44) (1483) 401-800 (UK), (81)(45) 341-7220 (Japan), or your nearest Silvaco distributor.

Simulation Standard, TCADDrivenCAD, Virtual Wafer Fab, Analog Alliance, Legacy, ATHENA, ATLAS, FAST ATLAS, ODIN, VYPER, TSUNAMI, RESILIENCE, TEMPEST, CELEBRITY, Manufacturing Tools, Automation Tools, Interactive Tools, TonyPlot, DeckBuild, DevEdit, Interpreter, ATHENA Interpreter, ATLAS Interpreter, Circuit Optimizer, MaskViews, PSTATS, SSuprem3, SSuprem4, Elite, Optolith, Flash, Silicides, SPDB, CMP, MC Deposit, MC Implant, Process Adaptive Meshing, S-Pisces, Blaze, Device 3D, Thermal 3D, Interconnect 3D, TFT, Luminous, Giga, MixedMode, ESD, Laser, FastBlaze, FastMixedMode, FastGiga, FastNoise, UTMOST, UTMOST II, UTMOST III, UTMOST IV, PROMOST, SPAYN, SmartSpice, MixSim, Twister, FastSpice, SmartLib, SDDL, EXACT, CLEVER, STELLAR, HIPEX, Scholar, SIREN, ESCORT, STARLET, Expert, Savage, Scout, Guardian and Envoy are trademarks of Silvaco International.

Hints, Tips and Solutions

Andy Strachan, Applications and Support Manager

Q: What are the options for generating 3D structures for ATLAS device simulation?

Currently there are three options for generating 3D device structures. In all cases the prismatic meshing of ATLAS/DEVICE3D permits arbitrary shaped device regions in 2 dimensions (typically X and Y) and rectangular regions in the other dimension (typically Z).

- **definition through the ATLAS syntax.** This limits the user to defining box shaped regions. Region definition is through statements such as:

```
region num=1 silicon x.min=0 \ x.max=1 y.min=0  
y.max=1 z.min=0 \ z.max=1
```

Mesh generation is handled through the Z.MESH statement which is analogous to the X.MESH and Y.MESH statement used in 2D ATLAS simulations. Electrodes and doping can be defined using the same syntax as 2D ATLAS but with Z.MIN and Z.MAX parameters to control the Z extent. Doping profiles can be read from the formats supported in 2D ATLAS: `ssuprem3`, `athena`, `ascii`.

- **use DEVEDIT3D to create a 3D mesh structure**
DEVEDIT3D is a 3D structure generation and meshing tool used to generate the mesh, regions, electrodes and doping used in ATLAS/DEVICE3D. It allows users to draw regions by hand in 2D and project them into the third direction. DEVEDIT3D contains all the sophisticated meshing options available to 2D DEVEDIT. These include: mesh constraints by region, mesh constraints by a user defined box, refinement on doping and other quantities, mouse controlled refine and unrefine boxes. DEVEDIT3D has both interactive and batch mode operation. This is the recommended approach for 3D power device simulation.
- **use ATHENA and DEVEDIT3D to extend a 2D process simulation to 3D**
A 2D process simulation from ATHENA can be extruded to form a 3D structure using DEVEDIT3D. In this mode DEVEDIT3D can be used to add extra regions and doping if required. This mode is commonly used for modeling MOS width effects in 3D (see Figure 1). An ATHENA simulation of the isolation bird's beak and field stop implant is performed. The 2D structure is loaded into DEVEDIT3D and extended in Z direction. The polysilicon gate is truncated in Z and aluminum source/drain contacts are added. The source/drain doping profiles can be

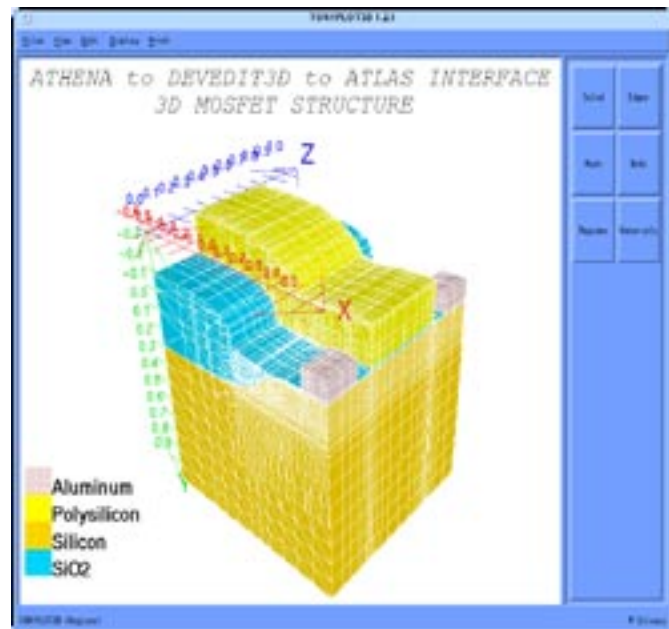


Figure 1. 3D device simulation of MOS width effect can be performed on structures created ATHENA.

read from analytical functions or other process simulation results. A worked example named `mos2ex04.in` is supplied with the Fall 96 release CDROM.

For devices with non-rectangular regions in the XZ plane such as pillar MOSFETs or cylindrically designed power structures DEVEDIT3D can also be used by drawing in the XZ plane and projecting into the Y direction.

The future release of Silvaco's 3D process/device simulator ODIN will provide a fourth option for 3D simulation problems. ODIN is based on tetrahedral mesh elements and will overcome the mesh restrictions described above.

Call for Questions

If you have hints, tips, solutions or questions to contribute, please contact our Applications and Support Department
Phone: (408) 567-1000 Fax: (408) 496-6080
e-mail: support@silvaco.com

Hints, Tips and Solutions Archive

Check our our Web Page to see more details of this example plus an archive of previous Hints, Tips, and Solutions
<http://www.silvaco.com>



SILVACO WANTS YOU!!

- **Spice Application Engineers**
- **Process and Device Application Engineers**

fax your resume to:
408-496-6080, or
e-mail to:
personnel@silvaco.com

Opportunities worldwide for apps engineers: Santa Clara, Phoenix, Austin, Boston, Tokyo, Guildford, Munich, Grenoble, Seoul, Hsinchu. Opportunities for developers at our California headquarters.

SILVACO 
International

4701 Patrick Henry Drive, Building 2
Santa Clara, CA 95054

Telephone: (408) 567-1000
Fax: (408) 496-6080
URL: <http://www.silvaco.com>